Nonlinear Oscillations of Suspended Cables Containing a Two-to-One Internal Resonance

CHRISTOPHER L. LEE and NOEL C. PERKINS

Department of Mechanical Engineering and Applied Mechanics, The University of Michigan, Ann Arbor, MI 48109-2125, U.S.A.

(Received: 21 October 1991; accepted: 4 February 1992)

Abstract. The near-resonant response of suspended, elastic cables driven by planar excitation is investigated using a two degree-of-freedom model. The model captures the interaction of a symmetric in-plane mode and an out-of-plane mode with near commensurable natural frequencies in a 2:1 ratio. The modes are coupled through quadratic and cubic nonlinearities arising from nonlinear cable stretching. The existence and stability of periodic solutions are investigated using a second order perturbation analysis. The first order analysis shows that suspended cables may exhibit saturation and jump phenomena. The second order analysis, however, reveals that the cubic nonlinearities and higher order corrections disrupt saturation. The stable, steady state solutions for the second order analysis compare favorably with results obtained by numerically integrating the equations of motion.

Key words: Cables, modal interactions, perturbation analysis, saturation.

1. Introduction

Cables are used in engineering applications that demand lightweight, flexible, or easily deployable structural members or conductors. For example, cables are suitable for transmitting electrical or optical signals, tethering objects over long distances, and towing and mooring marine vessels. In addition, underwater instrumentation arrays are often supported by individual cables or multiple cable networks. The overall flexibility of the cable, however, may render it susceptible to performance impairing oscillations.

A historical review of cable dynamics, along with a summary of recent contributions specific to suspended cables, can be found in [1]–[3]. The prominent linear theory developed by Irvine and Caughey [4] describes the free vibration of a suspended cable about a planar equilibrium with small sag and horizontal supports. For linear motions, the in-plane response decouples from the out-of-plane response. Moreover, the in-plane response can be decomposed into vibration modes that are either symmetric or anti-symmetric with respect to the cable mid-span. The anti-symmetric in-plane modes and all of the out-of-plane modes are identical to those of a taut string. The symmetric in-plane modes are distinguished by the fact that they induce first-order dynamic cable stretching.

Hagedorn and Shafer [5] were the first to extend the (in-plane) linear theory to account for geometric nonlinearities. Free planar, nonlinear cable oscillations were further studied in [6]–[9]. Two degree-of-freedom models were proposed to study free nonplanar, nonlinear cable oscillations with [10] and without [11] internal resonance. Various one and two degree of freedom models, without internal resonance [12]–[14] and with internal resonance [15], have been used to examine forced nonlinear oscillations. A recent theoretical study [16] demonstrates the key role

Nonlinear Dynamics **3**: 465–490, 1992.

played by a two-to-one internal resonance in initiating non-planar response for cables subjected to support oscillations. Companion experiments [17] provide the first response measurements in support of a nonlinear theory of suspended cables.

Internal resonances are known to enhance modal coupling and may produce strongly coupled nonlinear response in multi-degree-of-freedom dynamical systems; see, for example, [18]–[20]. Such systems may exhibit complex behavior such as vibration saturation and periodically, aperiodically, or chaotically modulated response. An extensive bibliography on this subject is presented in [21]. Of particular importance to the current study is the saturation phenomena which has been studied in the context of beam structures [22], ships [23], and shells [24] which contain a specific class of quadratic nonlinearities and a two-to-one internal resonance. A simplified, quadratically nonlinear model is used to show that suspended cables may also exhibit saturation [25]. Second order nonlinear cable stretching, however, is neglected. Experimental confirmation of vibration saturation was first reported by Haddow *et al.* [22].

This study focuses on the near-resonant response of suspended, elastic cables driven by planar excitation in the presence of a two-to-one internal resonance. The investigation begins with the presentation of a geometrically nonlinear continuum cable model that describes three-dimensional response. An asymptotic form of the model, describing suspensions with small equilibrium curvature (sag) and horizontal supports, is discretized using the Galerkin method. A two-degree-of-freedom discrete model is used to examine the coupling between a symmetric in-plane mode and an out-of-plane mode. These modes are coupled through quadratic and cubic nonlinearities which originate from nonlinear cable stretching. Two-to-one internal resonances naturally arise for specific sag levels where the natural frequency of the in-plane mode is, approximately, twice that of the out-of-plane mode. Planar and non-planar response of the cable is examined for conditions near primary resonance of the in-plane mode.

A perturbation analysis is carried out to second nonlinear order to examine the existence and stability of weakly nonlinear periodic motions. At the first nonlinear order, the discrete model is shown to possess the particular quadratic nonlinear terms that lead to saturation. The analysis is extended to second nonlinear order to capture the additional effects of the cubic nonlinearities and to include higher order corrections due to the quadratic nonlinearities. Examples illustrate that the saturation phenomena is disrupted and that higher order effects may qualitatively alter the nature of the steady state response. The accuracy of the higher order solutions are verified by comparison to results obtained by numerically integrating the equations of motion.

2. Theoretical Model

2.1. General Continuum Model

Figure 1 illustrates an elastic cable suspended between two level supports a distance H apart. The equilibrium cable (dotted curve) has length L and sags an amount D at the mid-span, due to gravity. Dynamic displacement of the cable from equilibrium (solid curve) is described by $\mathbf{U}(S, T) = U_1(S, T)\mathbf{l}_1 + U_2(S, T)\mathbf{l}_2 + U_3(S, T)\mathbf{l}_3$ where S represents the equilibrium arc length coordinate measured from the left support and T represents time. The unit vectors, $\mathbf{l}_1$, $\mathbf{l}_2$, and $\mathbf{l}_3$, define the tangential, normal, and bi-normal directions with respect to the equilibrium configuration.

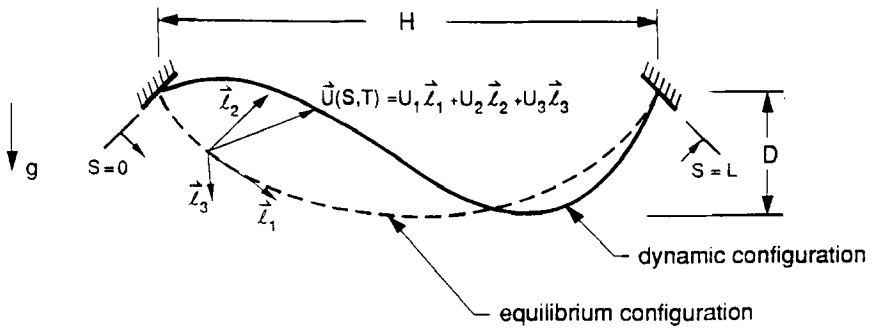

Fig. 1. An elastic cable, length L, is suspended between horizontal supports a distance H apart and has sag D at the mid-span. U describes three-dimensional displacement from the equilibrium configuration and is referred to the Frenet triad $(\mathbf{l}_1, \mathbf{l}_2, \mathbf{l}_3)$. Equilibrium configuration: dashed curve; dynamic configuration: solid curve.

Following [26], the nonlinear equations of motion are derived from Hamilton's principle under the following assumptions.

1. The cable is a homogeneous, one-dimensional elastic continuum obeying a linear stress-strain relationship.
2. Axial extensions of the cable are described by the Lagrangian strain of the centerline.
3. The flexural, torsional, and shear rigidities of the cable are negligible.

The nondimensional equations describing motion about the equilibrium are [26]

tangential direction,

$$[v_t^2 p(u_{1,s} - ku_2) + v_l^2(1 + u_{1,s} - ku_2)e]_{,s} - k[(v_t^2 p + v_l^2 e)(u_{2,s} + ku_1)] + f_1 = u_{1,tt}\,, \tag{1}$$

normal direction,

$$[(v_t^2 p + v_l^2 e)(u_{2,s} + ku_1)]_{,s} + k[v_l^2(1 + u_{1,s} - ku_2)e + v_t^2 p(u_{1,s} - ku_2)] + f_2 = u_{2,tt}\,, \tag{2}$$

bi-normal direction,

$$[(v_t^2 p + v_l^2 e)(u_{3,s})]_{,s} + f_3 = u_{3,tt}\,, \tag{3}$$

where

$$e(s,t) = u_{1,s} - ku_2 + \frac{1}{2}[(u_{1,s} - ku_2)^2 + (u_{2,s} + ku_1)^2 + (u_{3,s})^2] \tag{4}$$

is the dynamic component of the Lagrangian strain and the boundary conditions are

$$u_i(0,t) = u_i(1,t) = 0\,, \qquad i = 1,2,3\,. \tag{5}$$

The following nondimensional quantities are used in (1)–(5):

$$s = \frac{S}{L}\,;\quad t = \frac{T}{\sqrt{L/g}}\,;\quad f_i = \frac{F_i}{\rho g L}\,,\quad u_i = \frac{U_i}{L}\,,\quad i = 1,2,3\,;$$

$$v_t^2 = \frac{P_0}{\rho g L}\,;\quad \text{and}\quad v_l^2 = \frac{EA}{\rho g L}\,, \tag{6}$$

where g is the gravitational constant, ρ is the cable mass/length, EA is the axial stiffness of the cable cross-section, P_0 is the equilibrium tension of the cable at the mid-span ($S = L/2$), and F_i are (possible) distributed dynamic force components. The constant coefficients, v_t and v_l, represent the nondimensional propagation speed of transverse and longitudinal waves, respectively. The non-constant coefficients, $k(s)$ and $p(s)$, represent the equilibrium curvature and tension of the classical catenary and are given by

$$p(s) = \frac{[(v_t^2)^2 + (s - \frac{1}{2})^2]^{1/2}}{v_t^2} \quad \text{and} \quad k(s) = \frac{v_t^2}{(v_t^2)^2 + (s - \frac{1}{2})^2} . \tag{7}$$

Note that the equations of in-plane motion (1) and (2) are coupled through *linear* terms proportional to the equilibrium curvature. Furthermore, the in-plane and out-of-plane equations (1)–(3) are coupled through quadratic and cubic nonlinear terms which arise from nonlinear stretching (4). The quadratic nonlinearities, which capture the softening (hardening) of the cable as it deflects towards (away from) the center of equilibrium curvature, vanish in the limit of zero equilibrium curvature ($k \to 0$). In this limit, (1)–(5) describe the nonlinear response of a taut string.

2.2. *Asymptotic Model for Small Curvature*

In many applications, the cable supports substantial static tension ($P_0 \gg \rho g L$) and the resulting equilibrium curvature is small. In the small curvature regime, $D/H < 1/8$ [4], the catenary is well approximated by a parabola and the equilibrium tension and curvature (7) are constant to first order in the small curvature parameter k:

$$p \approx 1 \quad \text{and} \quad k \approx \frac{1}{v_t^2} = 8\frac{D}{H} . \tag{8}$$

Substituting (8) into (1)–(4) and neglecting terms on the order of k^2 or smaller, leads to:

tangential direction

$$[v_l^2 e]_{,s} = u_{1,tt} , \tag{9}$$

normal direction

$$[(v_t^2 + v_l^2 e)u_{2,s}]_{,s} + k v_l^2 e + F_2(s)\cos\Omega t = u_{2,tt} , \tag{10}$$

bi-normal direction

$$[(v_t^2 + v_l^2 e)u_{3,s}]_{,s} = u_{3,tt} , \tag{11}$$

with

$$e(s, t) = u_{1,s} - k u_2 + \frac{1}{2}[(u_{2,s})^2 + (u_{3,s})^2] , \tag{12}$$

where harmonic excitation in the normal direction is considered: $f_2 = F_2(s)\cos\Omega t$, $f_1 = f_3 = 0$.

As detailed in [4], longitudinal waves propagate along the cable with a speed (v_l) that is orders of magnitude greater than that associated with transverse waves (v_t); i.e., $v_t^2/v_l^2 \leq k$. Consequently, on the time scale of lower frequency transverse motions, the stretching of the cable occurs nearly instantaneously or *quasi-statically*. Employing this assumption, the longitudinal inertia term in (9) is neglected resulting in spatially uniform dynamic tension:

$$[v_l^2 e]_{,s} = 0 . \tag{13}$$

Integrating (13) twice and using (12) leads to

$$u_1(s, t) = g(t)s + \int_0^s \left\{ ku_2 - \frac{1}{2}\left[(u_{2,s})^2 + (u_{3,s})^2\right] \right\} d\eta + h(t) , \tag{14}$$

where the two functions of integration $g(t)$ and $h(t)$ are determined from application of the boundary conditions $u_1(0, t) = u_1(1, t) = 0$:

$$h(t) = 0$$

$$v_l^2 e = g(t) = \int_0^1 \left\{ -ku_2 + \frac{1}{2}\left[(u_{2,s})^2 + (u_{3,s})^2\right] \right\} d\eta . \tag{15}$$

Thus, the tangential component, u_1, which is of order k, is formally eliminated as an unknown. Substituting (15) and (8) into (10) and (11) leads to the following equations of transverse motion:

$$[v_t^2 + v_l^2 g(t)]u_{2,ss} + \frac{v_l^2}{v_t^2} g(t) + F_2(s) \cos \Omega t = u_{2,tt} \tag{16}$$

$$[v_t^2 + v_l^2 g(t)]u_{3,ss} = u_{3,tt} . \tag{17}$$

with the boundary conditions (5).

Equations (14)–(17) and (5) are an asymptotic form of the equations of three-dimensional motion and are valid in the limit of small equilibrium curvature. In (16) and (17), the term $[v_t^2 + v_l^2 g(t)]$ represents the overall cable tension comprising a static component, v_t^2, and a dynamic component, $v_l^2 g(t)$. This asymptotic model represents a nonlinear extension of Irvine and Caughey's linear theory [4]. Upon linearization, the equations (15)–(17), for free response, provide the natural frequencies and mode shapes of a suspended elastic cable as given in [4] and reviewed in Appendix A. These modes form the basis for the following discretization.

2.3. Discrete Model

Coupled in-plane and out-of-plane cable motion is investigated using a two-degree-of-freedom model. The asymptotic model for transverse response (15)–(17) is discretized using the separable solutions

$$u_2(s, t) = \theta_{1i}(s)\alpha_1(t) \quad \text{and} \quad u_3(s, t) = \theta_{2k}(s)\beta_2(t) , \tag{18}$$

where $\theta_{1i}(s)$ and $\theta_{2k}(s)$ are the ith and kth in-plane and out-of-plane cable mode shapes with natural frequencies ω_1 and ω_2, respectively; refer to Appendix A.

Substitution of (18) into (15)–(17) and application of the Galerkin method leads to the discrete model

$$\ddot{\alpha}_1 + 2\zeta_1\omega_1\dot{\alpha}_1 + \omega_1^2\alpha_1 + A_2\alpha_1^2 + A_3\alpha_1^3 + A_4\beta_2^2 + A_5\alpha_1\beta_2^2 = \hat{F}\cos(\Omega t)\,, \tag{19}$$

$$\ddot{\beta}_2 + 2\zeta_2\omega_2\dot{\beta}_2 + \omega_2^2\beta_2 + B_2\beta_2^3 + B_3\alpha_1\beta_2 + B_4\alpha_1^2\beta_2 = 0\,, \tag{20}$$

where modal damping terms have been introduced. The coefficients in (19) and (20) are defined in Appendix B. There, it is noted that the coefficients of the quadratic nonlinear terms vanish if θ_{1i} is taken to be an anti-symmetric mode. For a symmetric mode, however, these coefficients are never zero for nonzero equilibrium curvature ($k \neq 0$). Furthermore, the quadratic terms with the coefficients A_4 and B_3 enhance modal coupling whenever the frequency of the in-plane mode is, approximately, twice that of the out-of-plane mode; i.e. $\omega_1 \approx 2\omega_2$. This two-to-one frequency ratio occurs naturally for the suspended cable near any of the 'cross-over' points noted by Irvine and Caughey [4]; refer to Figure A1.

3. Perturbation Analysis

Periodic solutions to (19)–(20) are found for weakly nonlinear response near primary resonance of the in-plane mode. Solutions will be determined up to second (cubic) nonlinear order using a generalization of the method of multiple scales developed in [27].

Accordingly, the new independent time scales

$$T_n = \epsilon^n\Omega t \qquad n = 0, 1, 2, \ldots \tag{21}$$

are introduced where ϵ represents a small positive parameter and T_n, $n = 1, 2, \ldots$ are 'slow' time scales which capture the response due to the nonlinearities, damping, and external excitation. To second nonlinear order, $O(\epsilon^3)$, the displacements are represented by three-term uniform expansion in the new time scales:

$$\alpha_1(T;\epsilon) = \sum_{n=1}^{3} \epsilon^n\alpha_{1n}(T_0, T_1, T_2) \quad \text{and} \quad \beta_2(T;\epsilon) = \sum_{n=1}^{3} \epsilon^n\beta_{2n}(T_0, T_1, T_2)\,. \tag{22}$$

Ordering the excitation and damping terms so that they first appear at the first nonlinear order, $O(\epsilon^2)$, the excitation frequency and the damping coefficients are expanded as [27]:

$$\Omega^2 = \omega_1^2 + \epsilon\sigma = \omega_1^2 + \epsilon(\sigma_1 + \epsilon\sigma_2) \tag{23}$$

$$2\zeta_1\omega_1\Omega = \epsilon\mu_1 = \epsilon(\mu_{11} + \epsilon\mu_{12}) \tag{24}$$

$$2\zeta_2\omega_2\Omega = \epsilon\mu_2 = \epsilon(\mu_{21} + \epsilon\mu_{22})\,. \tag{25}$$

Similarly, the excitation amplitude is expanded as:

$$\hat{F} = \epsilon^2 F = \epsilon^2(f_1 + \epsilon f_2)\,. \tag{26}$$

The quantities σ_n, μ_{1n}, μ_{2n}, and f_n $(n = 1, 2)$ are used in (23)–(26) to introduce external detuning, damping, and excitation at each nonlinear order. They are combined as shown to form the overall external detuning, damping, and excitation parameters given, respectively, by σ, μ_1, μ_2, and F. Near a cross-over point, the natural frequency of a symmetric in-plane mode is nearly twice that of an out-of-plane mode. This relationship is expressed by

$$2\omega_2 = \omega_1 + \epsilon\rho = \omega_1 + \epsilon(\rho_1 + \epsilon\rho_2)\,, \tag{27}$$

where ρ is an overall internal detuning parameter.

Substituting (21)–(26) into (19) and (20), defining $\eta = \omega_2/\omega_1$, and collecting terms with like powers of ϵ, leads to the zeroth, first, and second nonlinear order equations below.

$O(\epsilon^1)$, *zeroth nonlinear order (linear)*:

$$\begin{aligned} &D_0^2\alpha_{11} + \alpha_{11}^2 = 0\,,\\ &D_0^2\beta_{21} + \eta^2\beta_{21} = 0\,. \end{aligned} \tag{28}$$

$O(\epsilon^2)$, *first nonlinear order (quadratic)*:

$$D_0^2\alpha_{12} + \alpha_{12} = -2D_0D_1\alpha_{11} - \frac{\sigma_1}{\omega_1^2}\,D_0^2\alpha_{11} - \frac{\mu_{11}}{\omega_1^2}\,D_0\alpha_{11} - \frac{A_2}{\omega_1^2}\,\alpha_{11}^2 - \frac{A_4}{\omega_1^2}\,\beta_{21}^2 + \frac{1}{2}\,\frac{f_1}{\omega_1^2}\,e^{iT_0} + cc\,,$$

$$D_0^2\beta_{22} + \eta^2\beta_{22} = -2D_0D_1\beta_{21} - \frac{\sigma_1}{\omega_1^2}\,D_0^2\beta_{21} - \frac{\mu_{21}}{\omega_1^2}\,D_0\beta_{21} - \frac{B_3}{\omega_1^2}\,\alpha_{11}\beta_{21} + cc\,. \tag{29}$$

$O(\epsilon^3)$, *second nonlinear order (cubic)*:

$$\begin{aligned} D_0^2\alpha_{13} + \alpha_{13} = {} & -2D_0D_1\alpha_{12} - (D_1^2 + 2D_0D_2)\alpha_{11} - \frac{\sigma_1}{\omega_1^2}\,(D_0^2\alpha_{12} + 2D_0D_1\alpha_{11})\\ & - \frac{\sigma_2}{\omega_1^2}\,D_0^2\alpha_{11} - \frac{\mu_{11}}{\omega_1^2}\,(D_0\alpha_{12} + D_1\alpha_{11}) - \frac{\mu_{12}}{\omega_1^2}\,D_0\alpha_{11}\\ & - \frac{2A_2}{\omega_1^2}\,\alpha_{11}\alpha_{12} - \frac{A_3}{\omega_1^2}\,\alpha_{11}^3 - \frac{2A_4}{\omega_1^2}\,\beta_{21}\beta_{22} - \frac{A_5}{\omega_1^2}\,\alpha_{11}\beta_{21}^2 + \frac{1}{2}\,\frac{f_2}{\omega_1^2}\,e^{iT_0} + cc\,,\\ D_0^2\beta_{23} + \eta^2\beta_{23} = {} & -2D_0D_1\beta_{22} - (D_1^2 + 2D_0D_2)\beta_{21} - \frac{\sigma_1}{\omega_1^2}\,(D_0^2\beta_{22} + 2D_0D_1\beta_{21})\\ & - \frac{\sigma_2}{\omega_1^2}\,D_0^2\beta_{21} - \frac{\mu_{21}}{\omega_1^2}\,(D_0\beta_{22} + D_1\beta_{21}) - \frac{\mu_{22}}{\omega_1^2}\,D_0\beta_{21}\\ & - \frac{B_2}{\omega_1^2}\,\beta_{21}^3 - \frac{B_3}{\omega_1^2}\,(\alpha_{11}\beta_{22} + \alpha_{12}\beta_{21}) - \frac{B_4}{\omega_1^2}\,\alpha_{11}^2\beta_{21} + cc\,, \end{aligned} \tag{30}$$

where $D_n = \partial/\partial T_n$, $n = 0,\ 1,\ 2$ and *cc* stands for the complex conjugate of the preceding terms.

Zeroth Order Expansion

The solution to (28) is

$$\alpha_{11}(T_1, T_2) = K_1(T_1, T_2)e^{iT_0} + cc \quad \text{and} \quad \beta_{21}(T_1, T_2) = K_2(T_1, T_2)e^{i\eta T_0} + cc\,, \tag{31}$$

where $K_n(T_1, T_2), n = 1, 2$ are slowly varying (complex) amplitudes determined by the following higher-order expansions.

First Order Expansion

Substitution of (31) into (29) leads to secular terms and small divisor terms which become secular in the presence of the internal resonance (27). Elimination of these secular terms leads to the two state equations

$$-2iD_1K_1 + \left(\frac{\sigma_1}{\omega_1^2} - i\,\frac{\mu_{11}}{\omega_1^2}\right)K_1 - \frac{A_4}{\omega_1^2}\,K_2^2 e^{i(\rho/\omega_1)T_1} + \frac{1}{2}\,\frac{f_1}{\omega_1^2} = 0\,, \tag{32}$$

$$-2i\eta D_1K_2 + \left(\frac{\sigma_1}{\omega_1^2}\,\eta^2 - i\,\frac{\mu_{21}}{\omega_1^2}\,\eta\right)K_2 - \frac{B_3}{\omega_1^2}\,K_1\bar{K}_2 e^{-i(\rho/\omega_1)T_1} = 0\,, \tag{33}$$

which govern the response of the (complex) amplitudes K_1 and K_2 on the time scale T_1. In (32) and (33), the overbar denotes a complex conjugate.

Introducing the polar form,

$$K_n = \frac{1}{2}\,a_n(T_1, T_2)e^{i\theta_n(T_1,T_2)}\,, \qquad n = 1, 2 \tag{34}$$

into (32) and (33) and separating these equations into real and imaginary parts results in the following four state equations,

$$a_1D_1\theta_1 + \frac{1}{2}\,\frac{\sigma_1}{\omega_1^2}\,a_1 - \frac{1}{4}\,\frac{A_4}{\omega_1^2}\,a_2^2\cos\gamma_1 + \frac{1}{2}\,\frac{f_1}{\omega_1^2}\cos\theta_1 = 0\,, \tag{35}$$

$$D_1a_1 + \frac{1}{2}\,\frac{\mu_{11}}{\omega_1^2}\,a_1 + \frac{1}{4}\,\frac{A_4}{\omega_1^2}\,a_2^2\sin\gamma_1 + \frac{1}{2}\,\frac{f_1}{\omega_1^2}\sin\theta_1 = 0\,, \tag{36}$$

$$\eta a_2D_1\theta_2 + \frac{1}{2}\,\frac{\sigma_1}{\omega_1^2}\,\eta^2a_2 - \frac{1}{4}\,\frac{B_3}{\omega_1^2}\,a_1a_2\cos\gamma_1 = 0\,, \tag{37}$$

$$\eta D_1a_2 + \frac{1}{2}\,\frac{\mu_{21}}{\omega_1^2}\,\eta a_2 - \frac{1}{4}\,\frac{B_3}{\omega_1^2}\,a_1a_2\sin\gamma_1 = 0\,, \tag{38}$$

where $\gamma_1 = 2\theta_2 - \theta_1 + (\rho/\omega_1)T_1$. The solutions to these state equations have been studied extensively and may exhibit the saturation phenomena; see, for example, [20] and [22]. *Therefore, to first nonlinear order, the suspended cable may also exhibit saturation* [25].

Steady state periodic solutions are fixed points of (35)–(38). At steady state, $D_1a_1 = D_1a_2 = D_1\theta_1 = 0$ and $D_1\theta_2 = -\rho/2\omega_1$ and (35)–(38) reduce to the algebraic equations,

$$a_1\sigma_1 = \frac{A_4}{2}\,a_2^2\cos\gamma_1 - f_1\cos\theta_1\,, \tag{39}$$

$$a_1\mu_{11} = -\frac{A_4}{2}\,a_2^2\sin\gamma_1 - f_1\sin\theta_1\,, \tag{40}$$

$$a_2\sigma_1 = \frac{1}{\eta^2}\left(\omega_2\rho a_2 + \frac{B_3}{2}\,a_1a_2\cos\gamma_1\right), \tag{41}$$

$$a_2\mu_{21} = \frac{B_3}{2\eta}\, a_1 a_2 \sin\gamma_1 \,, \tag{42}$$

which provide the steady state amplitudes and phases on the T_1 time scale. These solutions are reviewed in Appendix C. Complete discussions of the solutions and their stability are detailed in [22]. The perturbation analysis is now extended to second order in order to account for, (1) the contribution of the cubic nonlinearities, and (2) the higher order corrections due to the quadratic nonlinearities.

Second Order Expansion

Extending the perturbation analysis to second order requires finding the particular solutions to (29). After eliminating the secular terms, the particular solutions are

$$\alpha_{12} = \frac{A_2}{3\omega_1^2}\, K_1^2 e^{2iT_0} - \left(\frac{A_2}{\omega_1^2}\, K_1\bar{K}_1 + \frac{A_4}{\omega_1^2}\, K_2\bar{K}_2\right) + cc \,,$$

$$\beta_{22} = \frac{B_3}{\omega_1^2 + 2\omega_1\omega_2}\, K_1 K_2 e^{i(1+\eta)T_0} + cc \,. \tag{43}$$

Substituting (31) and (43) into (30) leads to equations for α_{13} and β_{23} which govern the variations of the (complex) amplitudes on the T_2 time scale. Elimination of the secular terms at this order requires

$$-D_1^2K_1 - 2iD_2K_1 - \left(2i\,\frac{\sigma_1}{\omega_1^2} + \frac{\mu_{11}}{\omega_1^2}\right)D_1K_1 + \left(\frac{\sigma_2}{\omega_1^2} - i\,\frac{\mu_{12}}{\omega_1^2}\right)K_1$$
$$+ 8\Lambda_1 K_1^2\bar{K}_1 + 8\Lambda_2 K_1K_2\bar{K}_2 + \frac{1}{2}\,\frac{f_2}{\omega_1^2} = 0 \,, \tag{44}$$

$$-D_1^2K_2 - 2i\eta D_2K_2 - \left(2i\,\frac{\sigma_1}{\omega_1^2}\,\eta + \frac{\mu_{21}}{\omega_1^2}\right)D_1K_2 + \left(\frac{\sigma_2}{\omega_1^2}\,\eta^2 - i\,\frac{\mu_{22}}{\omega_1^2}\,\eta\right)K_2$$
$$+ 8\Lambda_3 K_2^2\bar{K}_2 + 8\Lambda_4 K_1\bar{K}_1K_2 = 0 \,, \tag{45}$$

where

$$\Lambda_1 = \frac{1}{8\omega_1^4}\left(4A_2A_3 - \frac{2}{3}\,A_2^2 - 3A_3\omega_1^2\right), \quad \Lambda_2 = \frac{1}{8\omega_1^4}\left(4A_2A_4 - 2A_5\omega_1^2 - \frac{2A_4B_3\omega_1^2}{\omega_1^2 + 2\omega_1\omega_2}\right),$$

$$\Lambda_3 = \frac{1}{8\omega_1^4}\,(2A_4B_3 - 3B_2\omega_1^2), \quad \text{and} \quad \Lambda_4 = \frac{1}{8\omega_1^4}\left(2A_2B_3 - 2B_4\omega_1^2 - \frac{B_3^2\omega_1^2}{\omega_1^2 + 2\omega_1\omega_2}\right). \tag{46}$$

The above equations contain derivatives with respect to both T_1 and T_2 time scales. However, since those equations describe modulations on the T_2 time scale only, they should be taken to be independent of T_1[27]. Neglecting derivatives with respect to T_1, using (34), and separating the real and imaginary parts yields the amplitude and phase state equations

$$a_1D_2\theta_1 + \frac{1}{2}\,\frac{\sigma_2}{\omega_1^2}\,a_1 + \Lambda_1 a_1^3 + \Lambda_2 a_1 a_2^2 + \frac{1}{2}\,\frac{f_2}{\omega_1^2}\cos\theta_1 = 0 \tag{47}$$

$$D_2 a_1 + \frac{1}{2}\frac{\mu_{12}}{\omega_1^2} a_1 + \frac{1}{2}\frac{f_2}{\omega_1^2}\sin\theta_1 = 0 \tag{48}$$

$$\eta a_2 D_2\theta_2 + \frac{1}{2}\frac{\sigma_2}{\omega_1^2}\eta^2 a_2 + \Lambda_3 a_2^3 + \Lambda_4 a_1^2 a_2 = 0 \tag{49}$$

$$D_2 a_2 + \frac{1}{2}\frac{\mu_{22}}{\omega_1^2} a_2 = 0\,. \tag{50}$$

The algebraic equations governing steady state periodic motions on the T_2 time scale are

$$a_1\sigma_2 = -2\omega_1^2(\Lambda_1 a_1^3 + \Lambda_2 a_1 a_2^2) - f_2\cos\theta_1 \tag{51}$$

$$a_1\mu_{12} = -f_2\sin\theta_1 \tag{52}$$

$$a_2\sigma_2 = -\frac{2\omega_1^2}{\eta^2}(\Lambda_3 a_2^3 + \Lambda_4 a_1^2 a_2) \tag{53}$$

$$a_2\mu_{22} = 0\,. \tag{54}$$

Finally, combining (39)–(42) and (51)–(54) into (23)–(25) yields the algebraic equations governing steady-state oscillations on the original time scale T (to second nonlinear order):

$$a_1\Omega^2 = a_1\omega_1^2 + \epsilon\left(\frac{A_4}{2} a_2^2\cos\gamma_1\right) - \epsilon^2(2\omega_1^2)(\Lambda_1 a_1^3 + \Lambda_2 a_1 a_2^2) - \epsilon F\cos\theta_1 \tag{55}$$

$$a_1\mu_1 = -\frac{A_4}{2} a_2^2\sin\gamma_1 - F\sin\theta_1 \tag{56}$$

$$a_2\Omega^2 = a_2\omega_1^2 + \epsilon\left(\frac{1}{\eta^2}\right)\left(\omega_2\rho a_2 + \frac{B_3}{2} a_1 a_2\cos\gamma_1\right) - \epsilon^2\left(\frac{2\omega_1^2}{\eta^2}\right)(\Lambda_3 a_2^3 + \Lambda_4 a_1^2 a_2) \tag{57}$$

$$a_2\mu_2 = \frac{B_3}{2\eta} a_1 a_2\sin\gamma_1\,. \tag{58}$$

The equations above can be solved simultaneously for a_1, a_2, γ_1, and θ_1 for specified cable and excitation parameters. Note that the first order approximation (39)–(42) is recovered from (55)–(58) by neglecting terms of $O(\epsilon^2)$. As with the first order approximation, (55)–(58) admits two types of solutions: planar ($a_1 \neq 0$, $a_2 = 0$) and non-planar ($a_1 \neq 0, a_2 \neq 0$).

Planar Solution($a_2 = 0$)
Simultaneous solution of (55) and (56) leads to a cubic equation for a_1^2:

$$4\epsilon^2\omega_1^4\Lambda_1^2 a_1^6 + 4\epsilon\omega_1^2\Lambda_1\sigma a_1^4 + (\sigma^2 + \mu_1^2)a_1^2 - F^2 = 0 \tag{59}$$

and

$$\theta_1 = \tan^{-1}\left(\frac{\mu_1}{\sigma + 2\epsilon\omega_1^2\Lambda_1 a_1^2}\right) \tag{60}$$

to second nonlinear order. To first nonlinear order, (55) and (56) lead to a linear equation in a_1^2 and provide a solution for linear response. The second order approximation (59) results in a singular perturbation of the first order approximation; although, for small ϵ and/or small a_1 values, a_1 deviates little from the linear approximation. The stability of the periodic, planar solutions are determined by following the procedure described in Appendix D.

Non-Planar Solution

For this case, a_1, a_2, γ_1, and θ_1 are determined numerically from (55)–(58) using a hybrid Powell root finding algorithm. The stability of these solutions are determined by following the procedure described in Appendix D.

4. Results

A series of examples is presented to illustrate the major features of the periodic solutions. In all examples, solid (dashed) lines denote stable (unstable) periodic solutions obtained from the perturbation analysis. The diamonds represent results obtained by numerically integrating the equations of motion (19)–(20). The numerical integrations were performed using the ODEPACK subroutine LSODA [28]. After specifying initial conditions, the integration was carried out until the system reached steady state. This was deemed to have occurred when the peak-to-peak amplitudes over five consecutive excitation periods deviated by less than 0.1% from the average peak-to-peak amplitude during those five periods. Using an integration time step of $\Delta T = 0.1$, steady state typically occurred before $T = 30{,}000$. The in-plane oscillations were not centered about $a_1 = 0$. The quadratic nonlinearities in (19) cause the midpoint of the steady state oscillations to *drift* [20] from the equilibrium position toward the center of curvature of the equilibrium configuration.

4.1. Comparison of First Order and Second Order Expansions

The three examples given in this section highlight the key differences between the first order and the second order expansions. To facilitate a comparison with published results for the first order expansions, the system parameters are chosen to be similar to those used in [22]. Parameters specific to a suspended cable are considered in the example described in the following subsection.

The coefficients of the nonlinear terms used in all of the examples are given in Table I. For the first three examples, the coefficients of the quadratic nonlinearities responsible for saturation, A_4 and B_3, are identical to those used in [22].

TABLE I.
Coefficients of nonlinear terms

	Examples 1 & 2	Example 3	Suspended Cable
A_2	−6.00	−6.00	−121.761
A_3	−4.22	−39.78	100.145
A_4	−8.00	−8.00	−10.147
A_5	4.00	4.00	25.036
B_2	−5.33	−5.33	18.778
B_3	−4.00	−4.00	−60.881
B_4	−11.00	−315.00	75.109

The first example is distinguished by the damping and frequency parameters, $\zeta_1 = 0.04$, $\zeta_2 = 0.02$, $\omega_1 = 1.9999$, $\omega_2 = 1.0000$, and $\Omega = 1.9999$. Here, there is no external detuning and very little internal detuning, $\epsilon\rho = 0.0001$. Figure 2a shows the steady state amplitudes, a_1 and a_2, as functions of the excitation amplitude F as determined by the first order expansion. When $F \approx 63.99 \times 10^{-4}$, the stable response changes from a purely one degree-of-freedom motion to a strongly coupled, two degree-of-freedom motion in which the amplitude of the excited coordinate, a_1, *saturates* at the value $a_1^* = 2.0 \times 10^{-2}$. In contrast, the results of the second order expansion demonstrate that saturation does not occur; see Figure 2b. Instead of saturating, the amplitude a_1 slowly and monotonically increases as the excitation amplitude is increased. Thus, increases in excitation energy are distributed, to some degree, to *both* modes. The second order expansion

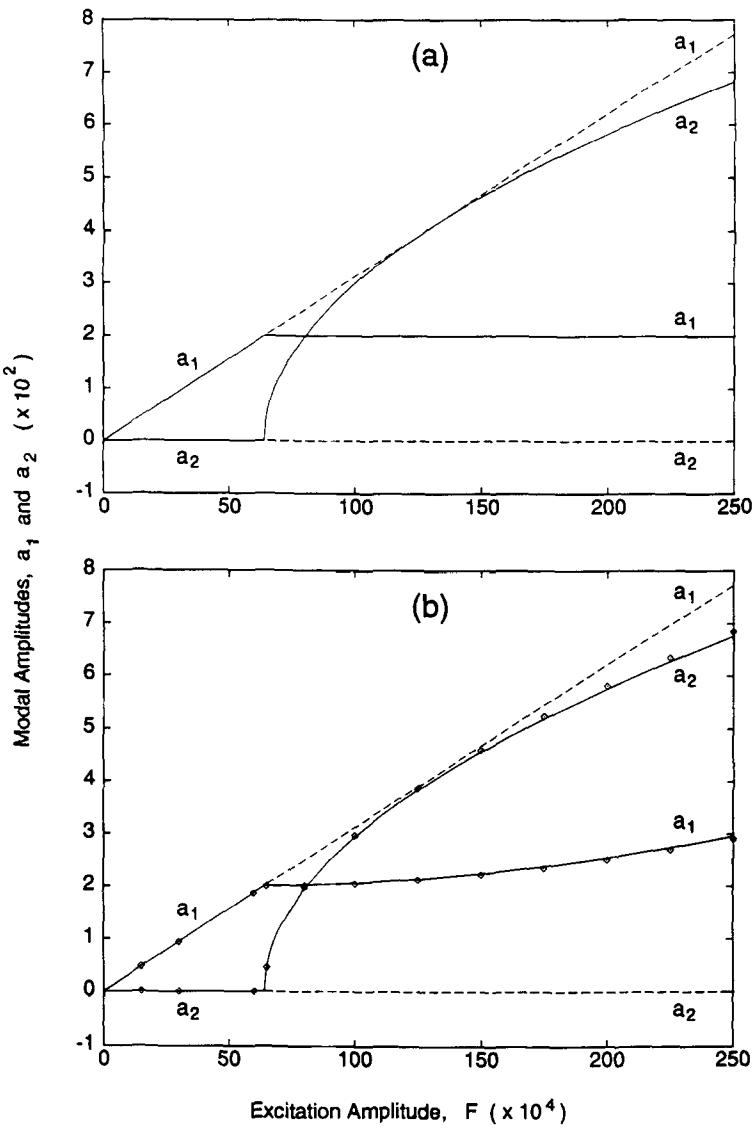

Fig. 2. Modal amplitudes (a_1, a_2) vs. excitation amplitude (F) for Example 1 with $\zeta_1 = 0.04$, $\zeta_2 = 0.02$, $\omega_1 = 1.9999$, $\omega_2 = 1.0000$, and $\Omega = 1.9999$. (a) First order expansion; (b) Second order expansion. Stable solutions: solid curves; unstable solutions: dashed curves; numerical results: diamonds.

also predicts that a slightly greater excitation level is required to initiate coupled response ($F = 64.00 \times 10^{-4}$). Note the overall good agreement between the results obtained by numerical integration and by the second order expansion.

In the second example, $\zeta_1 = 0.005$, $\zeta_2 = 0.0025$, $\omega_1 = 1.9999$, $\omega_2 = 1.0000$, and $\Omega = 2.0170$. Compared to the first example, the damping has been decreased by an order of magnitude and significant external detuning, $\epsilon\sigma = 0.069$, has been added. Results of the first order expansion, plotted in Figure 3a, illustrate both saturation and jump phenomena. For $5.22 \times 10^{-4} < F < 7.17 \times 10^{-4}$, two stable periodic solutions exist: one describing single degree-of-freedom response and the other describing coupled response. In this excitation range, a solution for a_1 describing unstable coupled response co-exists with the stable solution branch for a_1 at the saturation value,

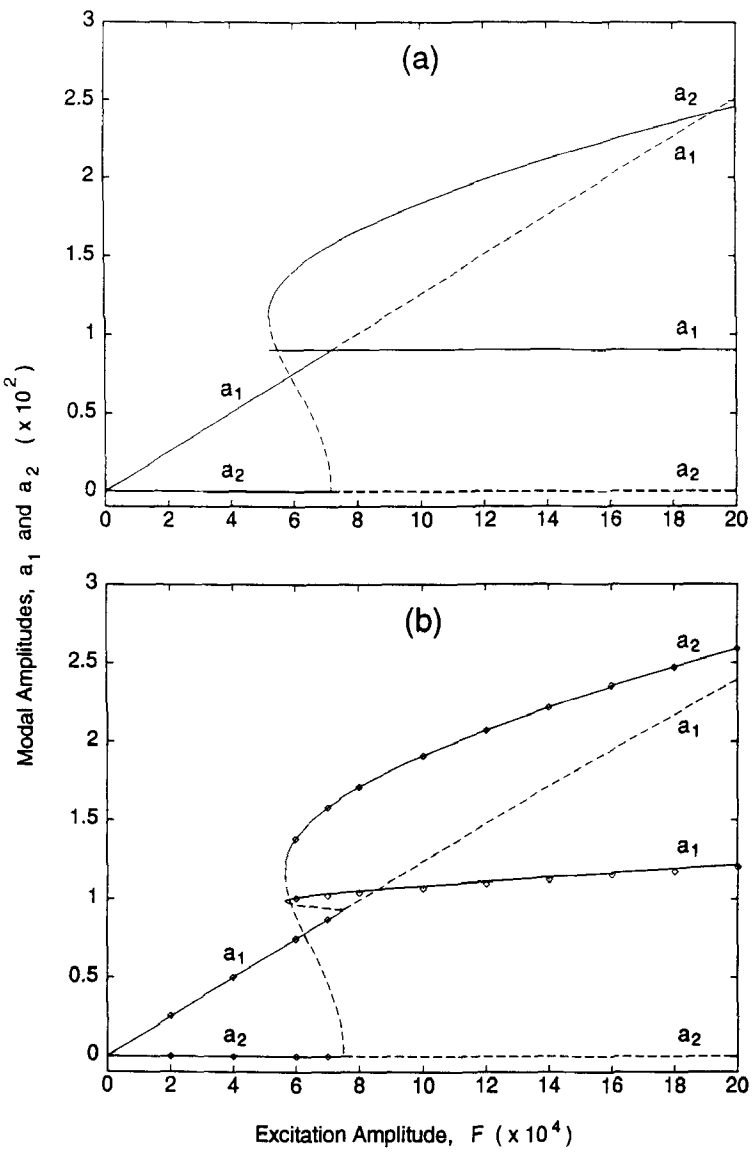

Fig. 3. Modal amplitudes (a_1, a_2) vs. excitation amplitude (F) for Example 2 with $\zeta_1 = 0.005$, $\zeta_2 = 0.00252$, $\omega_1 = 1.9999$, $\omega_2 = 1.0000$, and $\Omega = 2.0170$. (a) First order expansion; (b) Second order expansion. Stable solutions: solid curves; unstable solutions: dashed curves; numerical results: diamonds.

$a_1^* = 0.90 \times 10^{-2}$. In comparison to the first example, the coupled response now appears at a significantly lower excitation ($F = 5.22 \times 10^{-4}$) due to the decreased dissipation. Results for the second order expansion, shown in Figure 3b, again confirm that the amplitude of the directly excited mode, a_1, never saturates. Moreover, the second order expansion splits the (formerly degenerate) stable and unstable a_1 solution branches in the excitation range $5.22 \times 10^{-4} < F < 7.17 \times 10^{-4}$. It should be noted that for specific sets of parameters, the amplitude of the directly excited mode may decrease as the excitation amplitude is increased. This occurs for the present system if, for example, the external excitation frequency is $\Omega = 1.9800$ ($\epsilon\sigma = -0.079$).

Selected frequency-response results for the second example are illustrated in Figure 4. The results of the first order expansion (Figure 4a) and the second order expansion (Figure 4b) were computed using $F = 0.001$ (refer to Figure 3). For the first order expansion, the single degree-of-freedom solution possesses an unstable resonant peak at $\Omega = \omega_1 = 1.9999$. This solution is stable away from resonance for $\Omega < 1.979$ and $\Omega > 2.021$. A stable coupled solution exists for the frequency range $1.965 < \Omega < 2.032$, which overlaps the stability region for the single degree-of-freedom solution. Thus, the two stable periodic solutions co-exist for $1.965 < \Omega < 1.979$ and $2.021 < \Omega < 2.032$. In these two frequency ranges, the stable and unstable solution branches for a_1 are degenerate. Furthermore, the internal resonance shifts the solution branches for the coupled response to the left, causing these solution branches to be asymmetric with respect to the resonance $\Omega = \omega_1$. The corresponding solution branches in Figure 4b for the second order expansion possess a greater degree of asymmetry and are shifted further to the left. Moreover, the stable and unstable a_1 solution branches are no longer degenerate in the frequency ranges noted above. Again, the results obtained by numerical integration compare favorably with those obtained by the second order expansion.

The stability of all periodic solutions are determined following the procedure in Appendix D. There, it is observed that, for the second order expansion, there may be up to two points where a coupled solution bifurcates from the single degree-of-freedom solution. This observation follows from the fact that (94) may admit up to two real solutions for a_{1b}^*, depending on the particular system parameters chosen. For the system parameters defined in the first two examples, two bifurcations exist. In Figures 2 and 3, however, the second bifurcations (not shown) are substantially delayed and do not appear until the excitation amplitude is on the order of $F \approx 10$.

This is not the case for the third example defined in Table I for which the coefficients A_3 and B_4 are greater in magnitude. This system is perfectly tuned, $\omega_1 = 2\omega_2 = 2.00$, and lightly damped, $\zeta_1 = 2\zeta_2 = 0.005$. Figure 5a illustrates the steady state amplitudes as functions of the excitation amplitude for the second order expansion in the case of vanishing external detuning ($\Omega = 2.00$). For $F < 5.15 \times 10^{-4}$, the response is qualitatively similar to that of Figure 2b. In particular, for the coupled response, the amplitude of the directly excited mode, a_1, does not saturate but increases slightly with increasing F. However, when the excitation amplitude is increased to $F = 5.15 \times 10^{-4}$, a second (unstable) coupled solution bifurcates from the single degree-of-freedom solution. *Moreover, at this bifurcation point, the single degree-of-freedom solution regains stability.* For $F > 5.15 \times 10^{-4}$, stable single and two degree-of-freedom solutions co-exist. The results of the second order expansion compare favorably with those obtained by numerical integration for the stable coupled solution but slightly underpredict the amplitude of the single degree-of-freedom solution beyond the second bifurcation point. Third and higher order expansions would 'soften' the perturbation solution and improve the approximation. *It is emphasized here that the first order approximation cannot predict* (1) *the existence of the second bifurcation, and* (2) *the subsequent re-stabilization of the single degree-of-freedom periodic solution.*

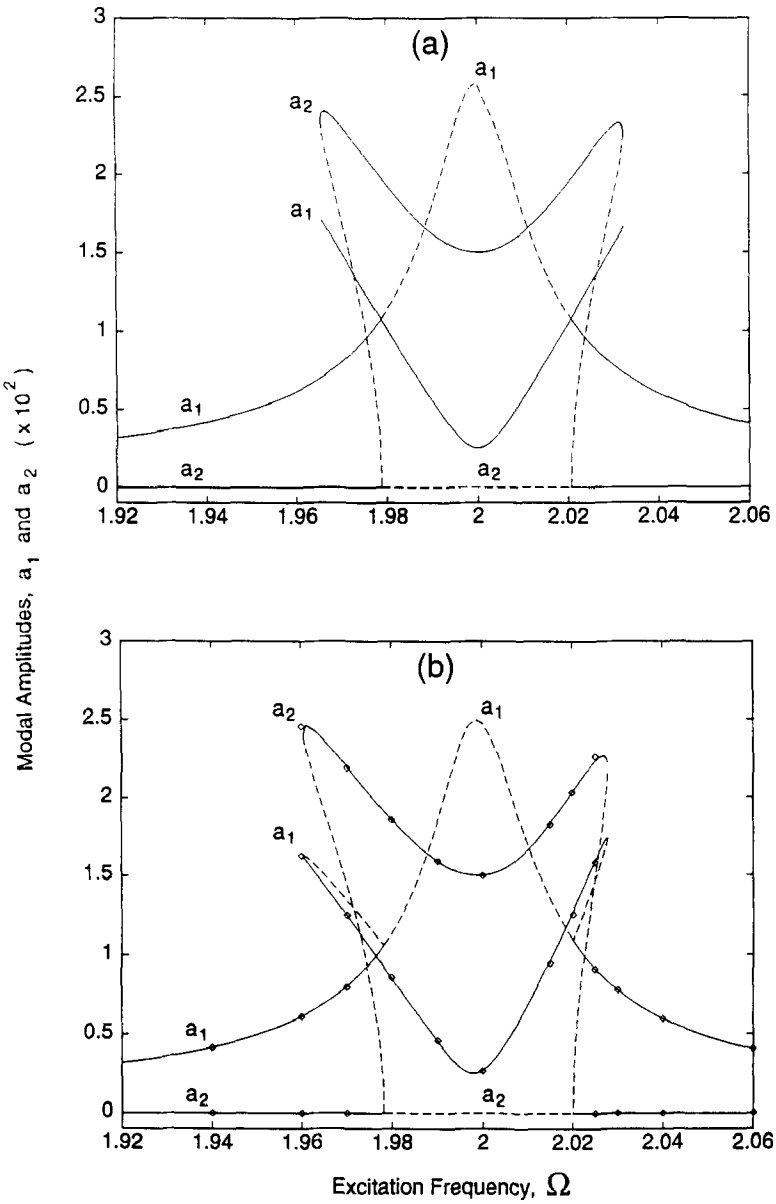

Fig. 4. Modal amplitudes (a_1, a_2) vs. excitation amplitude (Ω) for Example 2 with $\zeta_1 = 0.005$, $\zeta_2 = 0.0025$, $\omega_1 = 1.9999$, $\omega_2 = 1.0000$, and $F = 0.001$. (a) First order expansion; (b) Second order expansion. Stable solutions: solid curves; unstable solutions: dashed curves; numerical results: diamonds.

Figure 5b illustrates an example frequency response solution for the third example system computed for $F = 6.00 \times 10^{-4}$. The solution branches for coupled response display a large degree of asymmetry with respect to the primary resonance $\Omega = \omega_1 = 2.00$. The single degree-of-freedom response remains stable at primary resonance in contrast to the example of Figure 4b.

Inspection of (46) reveals that both the quadratic and the cubic nonlinearities contribute to the second order corrections. For a system with quadratic nonlinearities only, the second order corrections will have the same form as (51)–(54) since Λ_n, $n = 1, 4 \neq 0$.

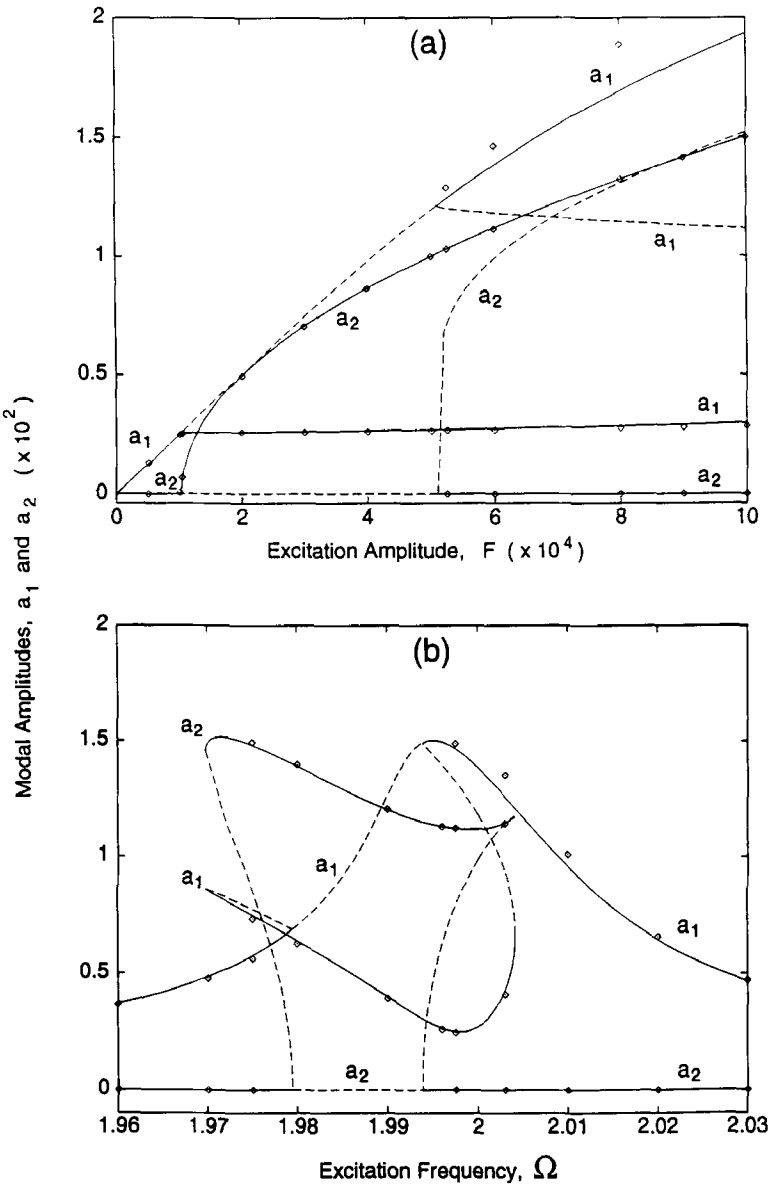

Fig. 5. Results of second order expansion for Example 3 with $\zeta_1 = 2\zeta_2 = 0.005$ and $\omega_1 = 2\omega_2 = 2.00$. (a) Modal amplitudes (a_1, a_2) vs. excitation amplitude (F) with $\Omega = 2.00$; (b) Modal amplitudes vs. excitation frequency (Ω) with $F = 6.00 \times 10^{-4}$. Stable solutions: solid curves; unstable solutions: dashed curves; numerical results: diamonds.

4.2. A Suspended Cable Example

The above examples illustrate possible periodic solutions for a class of two degree-of-freedom dynamical systems governed by (19) and (20). The particular solution characteristics displayed depend strongly upon the system parameters. Parameters specific to a suspended cable are listed in Table I, and are measured from a cable used in recent experiments [17]. The cable considered is a small diameter woven nylon cord of length $L = 26.3\,\text{m}$, weight/length $\rho g = 0.117\text{N/m}$, and $EA = 1900\text{N}$. For a sag-to-span ratio $D/H = 1/10$ ($\lambda^2 \approx 4\pi^2, v_t^2 = 7.10, v_t^2 = 1.25$), the natural

frequencies $\omega_1 = 7.025$ and $\omega_2 = 3.512$ are in a two-to-one ratio. The damping coefficients considered are $\zeta_1 = 0.0007$ and $\zeta_2 = 0.00035$.

Figure 6a shows the steady state response amplitudes as functions of the excitation amplitude for the second order expansion, for the case of near resonant excitation frequency $\Omega = 7.015$. In the context of the oscillating cable, the single degree-of-freedom response describes motion lying purely in the equilibrium plane. The coupled response describes a steady non-planar whirling of the cable in which the in-plane (normal) motion completes two cycles for every one cycle of out-of-plane motion.

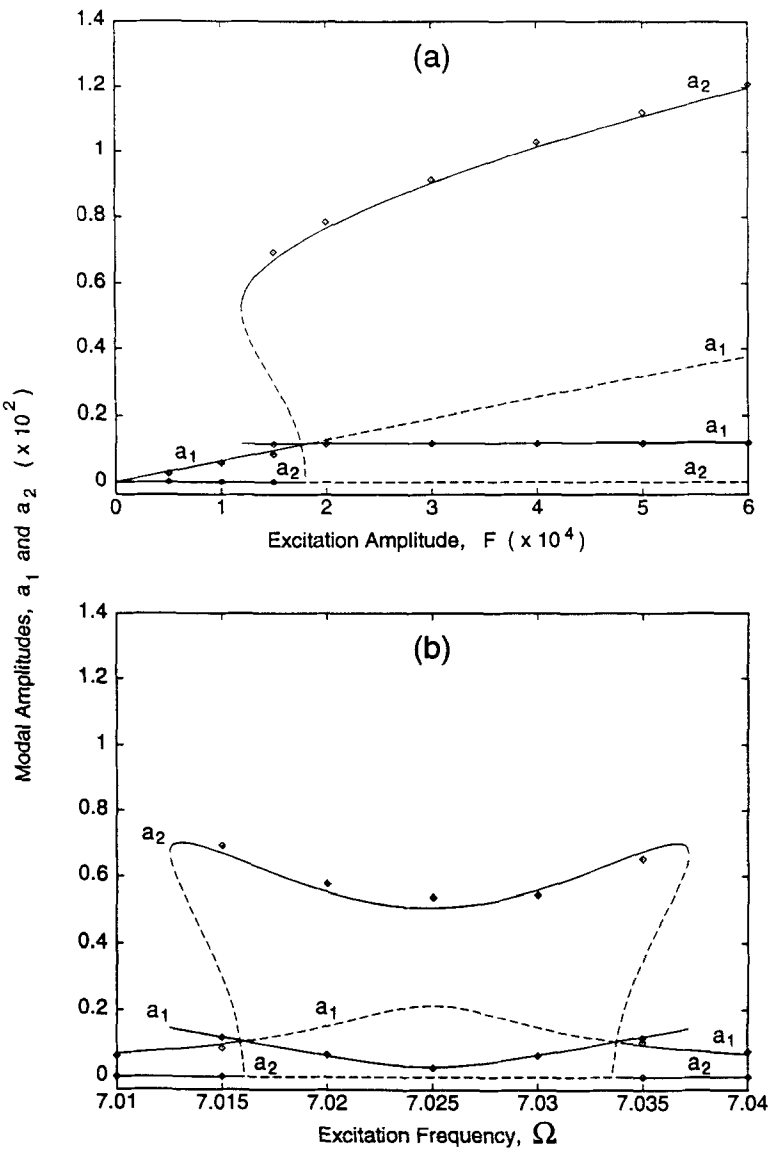

Fig. 6. Results of second order expansion for a suspended cable defined by $L = 26.3$ m, $\rho g = 0.117\,N$, $EA = 1900\,N$, $D/H = 1/10$. $\zeta_1 = 2\zeta_2 = 0.0007$ and $\omega_1 = 2\omega_2 = 7.025$. (a) Modal amplitudes (a_1, a_2) vs. excitation amplitude (F) with $\Omega = 7.015$; (b) Modal amplitudes vs. excitation frequency (Ω) with $F = 1.50 \times 10^{-4}$. Stable solutions: solid curves; unstable solutions: dashed curves; numerical results: diamonds.

As shown in Figure 6a, the cable executes planar response for (relatively) small excitation levels. The planar response looses stability at the first bifurcation ($F = 1.80 \times 10^{-4}$) and regains stability at the second bifurcation (not shown). In this example, the second bifurcation would occur at an extremely large excitation level ($F \approx 10$) which would render the weakly nonlinear assumption suspect. For excitation amplitudes above $F = 1.20 \times 10^{-4}$, the cable executes non-planar whirling similar to that generated experimentally by small support oscillations [17]. The second order expansion again predicts that the amplitude of the in-plane response a_1 increases (very) slowly with F. In the excitation region, $1.20 \times 10^{-4} < F < 1.80 \times 10^{-4}$, both planar and non-planar responses are stable. When $F < 1.80 \times 10^{-4}$, only the non-planar response is stable. The frequency response of the cable for the case $F = 1.50 \times 10^{-4}$ is shown in Figure 6b. Note that in the region about primary resonance, the stable periodic motion of the cable describes non-planar whirling. As with the previous examples, the second order expansion splits degenerate stable and unstable a_1 solution branches associated with the first order expansion. For the current example, however, the separation of these solution branches is extremely small.

5. Summary and Conclusion

A nonlinear continuum model of a suspended, elastic cable is presented which contains the quadratic and cubic nonlinear terms describing nonlinear cable stretching. An asymptotic form of this model is derived which is valid for suspensions having small equilibrium curvature. The asymptotic model is discretized using a symmetric in-plane mode and an out-of-plane mode. The resulting two degree-of-freedom model captures the modal interactions which arise when the natural frequency of the in-plane mode is nearly twice that of the out-of-plane mode. A perturbation analysis is used to determine periodic solutions and their stability for near resonant in-plane harmonic excitation.

A first order perturbation analysis confirms that the the quadratic nonlinearities lead to non-planar cable response exhibiting saturation and jump phenomena. Extending the perturbation analysis to second nonlinear order, however, reveals that saturation is disrupted by second order corrections associated with *both* the quadratic and the cubic nonlinear terms. Instead of saturating, the amplitude of the directly excited mode changes with excitation amplitude to a degree that depends strongly upon the system parameters. Moreover, the second order corrections split the degenerate periodic solutions predicted by the first order analysis. For the second order expansion, there may be up to two points where a non-planar solution bifurcates from a planar solution. In all of the examples presented, two bifurcation points exist and the planar solution regains stability beyond the second bifurcation. The accuracy of the second order analysis is validated through a comparison with results obtained by numerically integrating the equations of motion.

Acknowledgements

The authors gratefully acknowledge the support provided by the U.S. Office of Naval Research Young Investigator Program through grant number N00014-89-J-3159.

Appendix A: Linear Theory

From (15)–(17), the linearized equations of free motion about an equilibrium with small curvature (sag) are

$$u_{2,ss} - \lambda^2 \int_0^1 u_2 \, d\eta = \frac{1}{v_t^2} u_{2,tt} \tag{61}$$

and

$$u_{3,ss} = \frac{1}{v_t^2} u_{3,tt} , \tag{62}$$

with the boundary conditions

$$u_i(0, t) = u_i(1, t) = 0 , \qquad i = 2, 3 . \tag{63}$$

In (61), $\lambda^2 = v_l^2/(v_t^2)^3$ is the nondimensional cable parameter introduced by Irvine and Caughey [4] to characterize the geometry and elasticity of the cable. The solutions of the eigenvalue problems governing the in-plane and out-of-plane vibration are provided below.

In-Plane Vibration

The solution to the eigenvalue problem associated with (61) and (63) provides the natural frequencies and the normal component of the in-plane mode shapes. The mode shapes are either symmetric or anti-symmetric with respect to the mid-span of the cable ($s = \frac{1}{2}$).

The *symmetric* in-plane modes are

$$\theta_{1i}(s) = \frac{C_{1i}}{(\omega_1^2/v_t^2)} \left[1 - \tan\left(\frac{\omega_1}{2v_t}\right) \sin\left(\frac{\omega_1}{v_t} s\right) - \cos\left(\frac{\omega_1}{v_t} s\right) \right] \qquad i = 1, 3, 5, \ldots , \tag{64}$$

where C_{1i} is an arbitrary constant and ω_1 is the natural frequency determined by the characteristic equation

$$\left[\frac{(\omega_1/v_t)^3}{\lambda^2} - \frac{\omega_1}{v_t} \right] + 2 \tan\left(\frac{\omega_1}{2v_t}\right) = 0 . \tag{65}$$

The *anti-symmetric* in-plane modes are

$$\theta_{1j}(s) = C_{1j} \sin(j\pi s) , \qquad j = 2, 4, 6, \ldots , \tag{66}$$

where C_{1j} is an arbitrary constant. The natural frequencies are

$$\omega_1 = i\pi v_t , \qquad i = 2, 4, 6, \ldots . \tag{67}$$

In contrast to the symmetric modes, the anti-symmetric modes to not induce first order cable stretching and are the same as taut string modes.

Out-of-Plane Vibration

The eigenvalue problem associated with (62) and (63) is identical to that of a taut string and admits the eigensolutions

$$\theta_{2k} = C_{2k} \sin(k\pi s) , \qquad k = 1, 2, 3, \ldots \tag{68}$$

and

$$\omega_2 = k\pi v_t , \qquad k = 1, 2, 3, \ldots \tag{69}$$

Figure A1 illustrates the natural frequency spectrum of a suspended cable which depends solely on the cable parameter λ^2. The natural frequency loci of the symmetric in-plane modes (solid curves) strongly depend upon λ/π and 'cross-over' the natural frequency loci of the anti-symmetric in-plane modes (dashed curves) and the out-of-plane modes (dotted curves) which are both independent of λ/π. As discussed in [4], the suspended elastic cable model provides a smooth transition between the natural frequency spectra of a taut string ($\lambda/\pi \to 0$) and an inextensible cable ($\lambda/\pi \to \infty$).

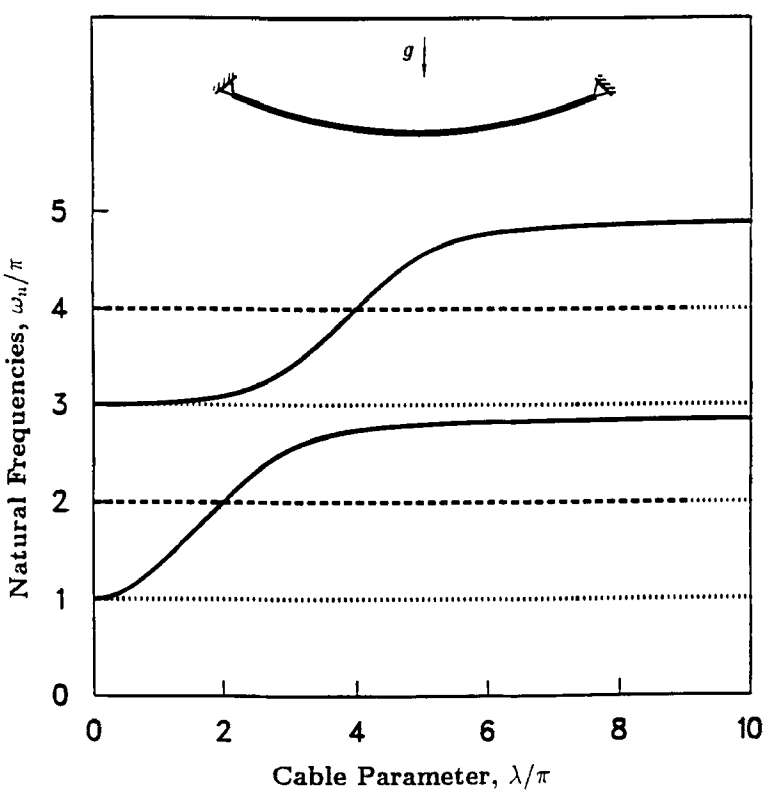

Fig. A1. Natural frequency spectrum for elastic cables with small sag and horizontal supports. Natural frequencies of the first four in-plane and out-of-plane modes are plotted vs. λ/π where λ^2 is a cable parameter [4]. Symmetric in-plane modes: solid curves; anti-symmetric in-plane modes: dashed curves; out-of-plane modes: dotted curves. The nth crossover occurs at $\lambda/\pi = 2n$, $n = 1, 2, \ldots$.

Appendix B: Coefficients of the Discrete Model

The coefficients of the discrete model (19) and (20) are

$$A_2 = -\frac{3}{2}\frac{v_l^2}{v_t^2}\frac{r_1 r_2}{r_4}, \quad A_3 = \frac{1}{2}v_l^2\frac{r_2^2}{r_4}, \quad A_4 = -\frac{1}{2}\frac{v_l^2}{v_t^2}\frac{r_1 r_3}{r_4}, \quad A_5 = \frac{1}{2}v_l^2\frac{r_2 r_3}{r_4},$$
$$B_2 = \frac{1}{2}v_l^2\frac{r_3^2}{r_5}, \quad B_3 = -\frac{v_l^2}{v_t^2}\frac{r_1 r_3}{r_5}, \quad B_4 = \frac{1}{2}v_l^2\frac{r_2 r_3}{r_5}, \quad \text{and} \quad \hat{F} = \frac{r_6}{r_4}, \tag{70}$$

where

$$r_1 = \int_0^1 \theta_{1i}\,ds, \quad r_2 = \int_0^1 \theta_{1i,s}^2\,ds, \quad r_3 = \int_0^1 \theta_{2k,s}^2\,ds,$$
$$r_4 = \int_0^1 \theta_{1i}^2\,ds, \quad r_5 = \int_0^1 \theta_{2k}^2\,ds, \quad \text{and} \quad r_6 = \int_0^1 \theta_{1i}F_2\,ds, \tag{71}$$

The vibration mode shapes θ_{1i} and θ_{2k} are given in Appendix A. Note that r_1 and the coefficients A_2, A_4, and B_3 would vanish if θ_{1i} was an anti-symmetric in-plane mode.

Appendix C: Solution to the First Order Expansion

For the first-order expansion (only), $f_1 = F$, $\mu_{11} = \mu_1$, $\mu_{21} = \mu_2$, and $\sigma_1 = \sigma$. Following [20] and [22] there are two sets of solutions, which in the context of the cable model, describe planar and non-planar responses.

Planar solution:
The planar solution,

$$a_1 = \pm\frac{F}{\sqrt{\sigma^2 + \mu_1^2}} \quad \text{and} \quad \theta_1 = \tan^{-1}(\mu_1/\sigma), \tag{72}$$

represents the linear response.

Non-planar solution:
The non-planar solution is given by

$$a_1 = \pm\frac{2}{B_3}\left[(\eta^2\sigma - \omega_2\rho)^2 + \eta^2\mu_2^2\right]^{1/2}, \tag{73}$$

$$a_2 = \pm\left[-\Gamma_1 \pm \left(\frac{4}{A_4^2}F^2 - \Gamma_2^2\right)^{1/2}\right]^{1/2}, \tag{74}$$

where

$$\Gamma_1 = \frac{4}{A_4 B_3} \left[\eta\mu_1\mu_2 - \sigma(\eta^2\sigma - \omega_2\rho)\right] \tag{75}$$

and

$$\Gamma_2^2 = \frac{16}{A_4^2 B_3^2} \left[\mu_1(\eta^2\sigma - \omega_2\rho) + \eta\mu_2\sigma\right]^2 \tag{76}$$

and

$$\theta_1 = \tan^{-1} \frac{\mu_1 a_1^2 + \dfrac{A_4}{B_3}\eta\mu_2 a_2^2}{\sigma a_1^2 - \dfrac{A_4}{B_3}(\eta^2\sigma - \omega_2\rho)a_2^2} \qquad \gamma_1 = \tan^{-1} \frac{\mu_2}{\eta\sigma - \omega_1\rho} \,. \tag{77}$$

The non-planar solution, which exists only for excitation amplitudes, $f_1 > \Upsilon_1$ where

$$\Upsilon_1 = \frac{1}{2} |A_4\Gamma_2| \,, \tag{78}$$

bifurcates from the planar solution at $f_1 = \Upsilon_2$ where

$$\Upsilon_2 = \frac{1}{2} |A_4| (\Gamma_1^2 + \Gamma_2^2)^{1/2} \,. \tag{79}$$

Note that for $f_1 > \Upsilon_1$, the in-plane amplitude, a_1, saturates at the value given by (73).

Appendix D: Stability Analysis

Planar Solution

The determination of planar stability begins with an expression for the modulation of the complex displacement amplitudes on the original time scale T:

$$\dot{K}_n = \epsilon D_1 K_n + \epsilon^2 D_2 K_n \,, \qquad n = 1, 2 \,. \tag{80}$$

Using (32)–(33) and (44)–(45), in (80) provides

$$2i\dot{K}_1 = \frac{\epsilon}{\omega_1^2}\left(\sigma K_1 - i\mu_1 K_1 - A_4 K_2^2 e^{i(\rho/\omega_1)T_1} + \frac{F}{2}\right) + 8\epsilon^2(\Lambda_1 K_1^2 \bar{K}_1 + \Lambda_2 K_1 K_2 \bar{K}_2) \tag{81}$$

$$2i\dot{K}_2 = \frac{\epsilon}{\omega_1^2}\left(\sigma\eta K_2 - i\mu_2 K_2 - \frac{B_3}{2\eta} K_1 \bar{K}_2 e^{-i(\rho/\omega_1)T_1}\right) + \frac{8\epsilon^2}{\eta}(\Lambda_3 K_2^2 \bar{K}_2 + \Lambda_4 K_1 \bar{K}_1 K_2) \,. \tag{82}$$

Let

$$K_1 = K_1^* + \delta K_1 \quad \text{and} \quad K_2 = \delta K_2 \tag{83}$$

where $(K_1^*, K_2^* = 0)$ is the steady state planar solution and δK_n, $n = 1, 2$ represent small perturbations. Substituting (83) into (81) and (82) and retaining linear terms in δK_n and $\delta \bar{K}_n$ leads to

$$i\delta \dot{K}_1 = R_1 \delta K_1 - iR_2 \delta K_1 + R_3 K_1^{*2} \delta \bar{K}_1 + 2R_3 K_1^* \bar{K}_1^* \delta K_1 , \tag{84}$$

$$i\delta \dot{K}_2 = S_1 \delta K_2 - iS_2 \delta K_2 - S_3 e^{-i(\rho/\omega_1)T_1} K_1^* \delta \bar{K}_2 + S_4 K_1^* \bar{K}_1^* \delta K_2 , \tag{85}$$

where

$$R_1 = \frac{\epsilon\sigma}{2\omega_1^2} , \quad R_2 = \frac{\epsilon\mu_1}{2\omega_1^2} , \quad R_3 = 4\epsilon^2 \Lambda_1 ,$$

$$S_1 = \frac{\epsilon\eta\sigma}{2\omega_1^2} , \quad S_2 = \frac{\epsilon\mu_2}{2\omega_1^2} , \quad S_3 = \frac{\epsilon B_3}{2\omega_1\omega_2} , \quad \text{and} \quad S_4 = \frac{4\epsilon^2}{\eta} \Lambda_4 . \tag{86}$$

Substitution of $K_1^* = a_1^* e^{i\theta_1^*}$ and

$$\delta K_1 = (B_{1r} + iB_{1i}) e^{i\theta_1^*} \quad \text{and} \quad \delta K_2 = (B_{2r} + iB_{2i}) e^{-i((\rho/2\omega_1)T_1 - (1/2)\theta_1^*)} , \tag{87}$$

where B_{nr} and B_{ni}, $n = 1, 2$ are real into (84) and (85) and separating real and imaginary terms yields:

$$\begin{aligned} &\dot{B}_{1i} + R_2 B_{1i} + \left[R_1 + \frac{3}{4} R_3 a_1^{*2} \right] B_{1r} = 0 \\ &\dot{B}_{1r} + R_2 B_{1r} + \left[-R_1 - \frac{1}{4} R_3 a_1^{*2} \right] B_{1i} = 0 \end{aligned} \tag{88}$$

and

$$\begin{aligned} &\dot{B}_{2i} + S_2 B_{2i} + \left[-\frac{1}{2} S_3 a_1^* + \left(S_1 - \frac{\epsilon}{2} \frac{\rho}{\omega_1} + \frac{1}{4} S_4 a_1^{*2} \right) \right] B_{2r} = 0 \\ &\dot{B}_{2r} + S_2 B_{2r} + \left[-\frac{1}{2} S_3 a_1^* + \left(S_1 - \frac{\epsilon}{2} \frac{\rho}{\omega_1} + \frac{1}{4} S_4 a_1^{*2} \right) \right] B_{2i} = 0 . \end{aligned} \tag{89}$$

Harmonic solutions

$$B_{nr} = b_{nr} e^{\lambda T_0} \quad \text{and} \quad B_{ni} = b_{ni} e^{\lambda T_0} , \qquad n = 1, 2 \tag{90}$$

exist provided the eigenvalues, λ, satisfy:

$$\lambda_{1,2} = -R_2 \pm \left[-\frac{3}{16} R_3^2 a_1^{*4} - R_1 R_3 a_1^{*2} - R_1^2 \right]^{1/2} , \tag{91}$$

$$\lambda_{3,4} = -S_2 \pm \left[\frac{1}{4} S_3^2 a_1^{*2} - \left(S_1 - \frac{\epsilon}{2} \frac{\rho}{\omega_1} + \frac{1}{4} S_4 a_1^{*2} \right)^2 \right]^{1/2} . \tag{92}$$

The eigenvalues $\lambda_{1,2}$ and $\lambda_{3,4}$, respectively, define the stability of the planar solution with

respect to perturbations in the in-plane (a_1) and out-of-plane (a_2) directions. The planar solution is stable if and only if $Re[\lambda_i] < 0$, $i = 1, 2, 3, 4$. Although stability could possibly be lost through a Hopf bifurcation, for the examples presented in this paper, it is observed that planar stability is always exchanged through either a turning point or a pitchfork bifurcation where either $\lambda_{1,2} = 0$ or $\lambda_{3,4} = 0$. Furthermore, when $\lambda_{3,4} = 0$ (pitchfork), a non-planar solution bifurcates from the planar solution. Thus, up to two distinct bifurcations of a non-planar solution from the planar solution may exist depending upon the system parameters.

The in-plane amplitude at a bifurcation point, a_{1b}^*, can be determined from either (91) or (92). Accordingly, a_{1b}^* satisfies either

$$\frac{3}{16} R_3^2 a_{1b}^{*4} + R_1 R_3 a_{1b}^{*2} + (R_1^2 + R_2^2) = 0 \qquad \text{or} \tag{93}$$

$$\frac{1}{16} S_4^2 a_{1b}^{*4} + \left[\frac{1}{2}\left(S_1 - \frac{\epsilon}{2}\frac{\rho}{\omega_1}\right)S_4 - \frac{1}{4} S_3^2\right] a_{1b}^{*2} + \left[\left(S_1 - \frac{\epsilon}{2}\frac{\rho}{\omega_1}\right)^2 + S_2^2\right] = 0 . \tag{94}$$

Only one bifurcation exists for the first order analysis; see for example [22]. The corresponding excitation amplitude or excitation frequency at a bifurcation can be found using (59).

Non-Planar Solution

In this case, the stability analysis begins with

$$\dot{a}_n = \epsilon D_1 a_n + \epsilon^2 D_2 a_n \quad \text{and} \quad \dot{\theta}_n = \epsilon D_1 \theta_n + \epsilon^2 D_2 \theta_n \qquad n = 1, 2 , \tag{95}$$

which describe the amplitude and phase modulations with respect to the original time scale T. Substituting (35)–(38) and (47)–(50), into (95) yields

$$\dot{a}_1 = -\frac{\epsilon}{2\omega_1^2}\left(\mu_1 a_1 + \frac{A_4}{2} a_2^2 \sin\gamma_1 + F \sin\theta_1\right), \tag{96}$$

$$a_1\dot{\theta}_1 = -\frac{\epsilon}{2\omega_1^2}\left(\sigma a_1 - \frac{A_4}{2} a_2^2 \cos\gamma_1 + F\cos\theta_1\right) - \epsilon^2(\Lambda_1 a_1^3 + \Lambda_2 a_1 a_2^2), \tag{97}$$

$$\dot{a}_2 = -\frac{\epsilon}{2\omega_1^2}\left(\mu_2 a_2 - \frac{B_3}{2\eta} a_1 a_2 \sin\gamma_1\right), \tag{98}$$

$$a_2\dot{\theta}_2 = -\frac{\epsilon}{2\omega_1^2}\left(\eta\sigma a_2 - \frac{B_3}{2\eta} a_1 a_2 \cos\gamma_1\right) - \frac{\epsilon^2}{\eta}(\Lambda_3 a_2^3 + \Lambda_4 a_1^2 a_2). \tag{99}$$

Using $\dot{\gamma}_1 = 2\dot{\theta}_2 - \dot{\theta}_1$ along with

$$a_n = a_n^* + \delta a_n \quad \text{and} \quad \theta_n = \theta_n^* + \delta\theta_n , \qquad n = 1, 2 , \tag{100}$$

where $(\,)^*$ denotes a steady state value and $\delta(\,)$ denotes a small perturbation, in (96)–(99) leads to the linear variational equations:

$$\delta\dot{a}_1 = -\frac{\epsilon}{2\omega_1^2}\left\{[\mu_1]\delta a_1 + [F\cos\theta_1^*]\delta\theta_1 + [A_4 a_2^* \sin\gamma_1^*]\delta a_2 + \left[\frac{A_4}{2} a_2^{*2}\cos\gamma_1^*\right]\delta\gamma_1\right\}, \tag{101}$$

$$\delta\dot{\theta}_1 = \frac{\epsilon}{2\omega_1^2}\left\{\left[F\frac{\cos\theta_1^*}{a_1^{*2}} - \frac{A_4}{2}\frac{a_2^{*2}\cos\gamma_1^*}{a_1^{*2}} - 4\epsilon\omega_1^2\Lambda_1 a_1^*\right]\delta a_1 + \left[F\frac{\sin\theta_1^*}{a_1^*}\right]\delta\theta_1 + \left[A_4\frac{a_2^*\cos\gamma_1^*}{a_1^*} - 4\epsilon\omega_1^2\Lambda_2 a_2^*\right]\delta a_2 + \left[-\frac{A_4}{2}\frac{a_2^{*2}\sin\gamma_1^*}{a_1^*}\right]\delta\gamma_1\right\}, \tag{102}$$

$$\delta\dot{a}_2 = \frac{\epsilon}{4\omega_1^2\eta}\{[B_3 a_2^*\sin\gamma_1^*]\delta a_1 + [-2\eta\mu_2 + B_3 a_1^*\sin\gamma_1^*]\delta a_2 + [B_3 a_1^* a_2^*\cos\gamma_1^*]\delta\gamma_1\}, \tag{103}$$

$$\delta\dot{\gamma}_1 = \left[\frac{\epsilon}{2\omega_1^2}\left\{\left(\frac{B_3}{\eta} + \frac{A_4}{2}\frac{a_2^{*2}}{a_1^{*2}}\right)\cos\gamma_1^* - F\frac{\cos\theta_1^*}{a_1^{*2}} + \epsilon\omega_1^2 a_1^*\left(4\Lambda_1 - \frac{8}{\eta}\Lambda_4\right)\right\}\right]\delta a_1 + \left[-\frac{\epsilon}{2\omega_1^2}F\frac{\sin\theta_1^*}{a_1^*}\right]\delta\theta_1 + \left[-\frac{\epsilon}{2\omega_1^2}A_4\frac{a_2^*\cos\gamma_1^*}{a_1^*} + 2\epsilon^2 a_2^*\left(\Lambda_2 - \frac{2}{\eta}\Lambda_3\right)\right]\delta a_2 + \left[\frac{\epsilon}{2\omega_1^2}\sin\gamma_1^*\left(\frac{A_4}{2}\frac{a_2^{*2}}{a_1^*} - \frac{B_3}{\eta}a_1^*\right)\right]\delta\gamma_1, \tag{104}$$

which can be written in the form

$$\{\dot{\mathbf{x}}\} = [A]\{\mathbf{x}\}, \tag{105}$$

where $\{\mathbf{x}\} = \{\delta a_1, \delta\theta_1, \delta a_2, \delta\gamma_1\}^T$.

The eigenvalues of $[A]$ govern stability of the non-planar solutions and are determined numerically. Note that stability of the planar solution cannot be assessed from equations (101)–(104) by simply setting $a_2^* = 0$; since, equations (103) and (104) vanish, decoupling the in-plane and out-of-plane motions.

References

1. Irvine, H. M., *Cable Structures*, MIT Press, Cambridge, 1981.
2. Triantafyllou, M. S., 'Linear dynamics of cables and chains', *Shock and Vibration Digest* **16**, 1984, 9–17.
3. Triantafyllou, M. S., 'Dynamics of cables and chains', *Shock and Vibration Digest* **19**, 1987, 3–5.
4. Irvine, H. M. and Caughey, T. K., 'The linear theory of free vibrations of a suspended cable', *Proceedings of the Royal Society of London* **A341**, 1974, 299–315.
5. Hagedorn, P. and Schafer, B., 'On non-linear free vibrations of an elastic cable', *International Journal of Non-Linear Mechanics* **15**, 1980, 333–340.
6. Rega, G. and Luongo, A., 'Natural vibrations of suspended cables with flexible supports', *Computers & Structures* **12**, 1980, 65–75.
7. Rega, G., Vestroni, F., and Benedettini, F., 'Parametric analysis of large amplitude free vibrations of a suspended cable', *International Journal of Solids and Structures* **20**, 1980, 95–105.
8. Luongo, A., Rega, G. and Vestroni, F., 'Planar non-linear free vibration of an elastic cable', *International Journal of Non-Linear Mechanics* **19**, 1984, 39–52.
9. Takahashi, K. and Konishi, Y., 'Nonlinear vibrations of cables in three dimensions, part I: nonlinear free vibrations', *Journal of Sound and Vibration* **118**, 1987, 69–84.
10. Benedettini, F., Rega, G. and Vestroni, F., 'Modal coupling in the free nonplanar finite motion of an elastic cable', *Meccanica* **21**, 1986, 38–46.
11. Luongo, A., Rega, G. and Vestroni, F., 'Monofrequent oscillations of a non-linear model of a suspended cable', *Journal of Sound and Vibration* **82**, 1982, 247–259.
12. Benedettini, F. and Rega, G., 'Nonlinear dynamics of an elastic cable under planar excitation', *International Journal of Non-Linear Mechanics* **22**, 1987, 497–509.

13. Takahashi, K. and Konishi, Y., 'Nonlinear vibrations of cables in three dimensions, part II: out-of-plane vibrations under in-plane sinusoidally time-varying load', *Journal of Sound and Vibration* **118**, 1987, 85–97.
14. Benedettini, F. and Rega, G., 'Numerical simulations of chaotic dynamics in a model of an elastic cable', *Nonlinear Dynamics* **1**, 1990, 23–38.
15. Rao, G. V. and Iyengar, R. N., 'Internal resonance and non-linear response of a cable under periodic excitation', *Journal of Sound and Vibration* **149**, 1991, 25–41.
16. Perkins, N. C., 'Planar and non-planar response of a suspended cable driven by small support oscillations', in *Proceedings First International Offshore and Polar Engineering Conference*, Edinburgh, U.K., Aug. 11–16, 1991, 210–215.
17. Perkins, N. C., 'Modal interactions in the nonlinear response of elastic cables under parametric/external excitation', *International Journal of Non-Linear Mechanics*, in press.
18. Miles, J. W., 'Stability of forced oscillations of a spherical pendulum', *Quarterly of Applied Mathematics* **20**, 1962, 21–32.
19. Sethna, P. R. and Bajaj, A. K., 'Bifurcations in dynamical systems with internal resonance', *Journal of Applied Mechanics* **45**, 1978, 895–902.
20. Nayfeh, A. H. and Mook, D. T., 1979, *Nonlinear Oscillations*, John Wiley, New York.
21. Nayfeh, A. H. and Balachandran, B., 'Modal interactions in dynamical and structural systems', *Applied Mechanics Review* **42**, 1989, S175–S202.
22. Haddow, A. G., Barr, A. D. S., and Mook, D. T., 'Theoretical and experimental study of modal interaction in a two-degree-of-freedom structure', *Journal of Sound and Vibration* **97**, 1984, 451–473.
23. Nayfeh, A. H., 'On the undesirable roll characteristics of ships in regular seas', *Journal of Ship Research* **32**, 1988, 92–100.
24. Nayfeh, A. H. and Raouf, R. A., 'Nonlinear oscillation of circular cylindrical shells', *International Journal of Solids and Structures* **23**, 1987, 1625–1638.
25. Tadjbakhsh, I. G. and Wang, Y. M., 'Wind-driven nonlinear oscillations of cables', *Nonlinear Dynamics* **1**, 1990, 265–291.
26. Perkins, N. C. and Mote, C. D., Jr., 'Three-dimensional vibration of travelling elastic cables', *Journal of Sound and Vibration* **114**, 1987, 325–240.
27. Rahman, Z. and Burton, T. D., 'On higher order methods of multiples scales in non-linear oscillations-periodic steady state response', *Journal of Sound and Vibration* **133**, 1989, 369–379.
28. Hindmarsh, A. C., 'ODEPACK, a systematized collection of ODE solvers', in *Scientific Computing* 1, R. S. Stepleman *et al.* (eds.) North Holland, Amsterdam, 1983, 55–64.